

Preparation of Iron-Doped SiO₂/TiO₂ Using Silica from Sugarcane Bagasse Ash for Visible Light Degradation of Congo Red

Nawwal Hikmah, Dewi Agustiniingsih, Nuryono Nuryono, and Eko Sri Kunarti*

Department of Chemistry, Faculty Mathematics and Natural Sciences, Universitas Gadjah Mada, Sekip Utara, PO BOX BLS 21, Yogyakarta 55281, Indonesia

* Corresponding author:

email: eko_kunarti@ugm.ac.id

Received: October 1, 2021

Accepted: November 9, 2021

DOI: 10.22146/ijc.69501

Abstract: Iron(III)-doped SiO₂/TiO₂ composite (SiO₂/TiO₂-Fe) has been prepared from sugarcane bagasse ash for photocatalytic degradation of Congo Red. This research was initiated by preparing SiO₂ from sugarcane bagasse ash through a sol-gel method. The SiO₂/TiO₂-Fe was obtained by mixing SiO₂ gel with TiO₂-Fe sol which was produced with titanium tetraisopropoxide (TTIP) as precursor and FeCl₃·H₂O as the dopant source. Dopant concentration was varied by 0, 1, 3, 5, 7% (w/w). The prepared materials were characterized by FT-IR, XRD, SR-UV, XRF, SAA, and SEM-EDX. The photocatalytic activity was evaluated for Congo Red degradation in a closed reactor under visible light illumination. The degradation yield was determined by the UV-Visible spectrophotometry method. Results showed that SiO₂ was successfully extracted from bagasse ash with a silica content of 90.87%. The SiO₂/TiO₂-Fe composite was successfully prepared with the bandgap energy value (E_g) decreasing as the dopant concentration increased. The optimum E_g of 2.63 eV was obtained at the concentration of Fe was 5%. Under that condition, the SiO₂/TiO₂-Fe photocatalyst degraded Congo Red solution by 98.18 % under visible light at pH 3 with a mass of 30 mg for 90 min. The SiO₂/TiO₂-Fe composite is expected to be a photocatalyst material candidate for dye wastewater treatment.

Keywords: sugarcane bagasse ash; SiO₂/TiO₂-Fe; photocatalyst; Congo Red; degradation

■ INTRODUCTION

Textile industry waste in the form of dyes has recently become an environmental problem because of its increasing amount of disposal. One of these dye wastes is Congo Red. The existence of Congo Red waste generates some toxic impacts which are able to disrupt the aquatic ecosystem. Its toxic effects include causing oxygen depletion and reducing the amount of light penetrated to alter the photosynthetic activity of some aquatic living organisms, and it is known as one of the carcinogenic chemicals. Consequently, it is highly required to overcome these environmental problems caused by Congo Red waste [1].

Several ways have been done to overcome dye waste, one of which is adsorption [2], coagulation [3], and ozonation [4]. However, the dye is only adsorbed in the adsorption method without being degraded, released, and becoming a secondary pollutant. The photocatalysis

method using a semiconductor photocatalyst could be applied to remove dye waste [5], degrading dyes into simpler, safer, and economic components.

Photocatalyst is a material that can absorb light and carry out some chemical transformations by redox reaction [6]. One photocatalyst material that is commonly used is titanium dioxide (TiO₂). TiO₂ has a high oxidation capacity, high photostability, and is non-toxicity [7]. Hence, TiO₂ is widely used as a photocatalyst material. However, TiO₂ has a small specific surface area and easily forms agglomeration between its particle and recombination between its charge carriers. This weakness can be overcome by dispersing TiO₂ into a porous material, such as silica (SiO₂) [8]. The SiO₂ can reduce TiO₂ particle size and minimize agglomeration between TiO₂ particles to increase the surface area and catalytic activity. The silica used can be extracted from natural materials with high

silica content [9]. Recent studies state that one of the natural materials that have the potential as a source of silica is bagasse which has a silica content of 88.68% [10]. However, the $\text{SiO}_2/\text{TiO}_2$ composite photocatalyst needs UV radiation (≤ 390 nm) for dye degradation because of the significant bandgap energy of TiO_2 .

Based on previous research, it is known that TiO_2 has a value of bandgap energy of 3.26 eV [11-13]. It allows TiO_2 to absorb only UV lights for dye waste treatment, limiting the application of TiO_2 on an industrial scale [13-17]. Besides, another limitation is that UV light takes less than 5% of solar light irradiated on the earth's surface [18]. Therefore, it is necessary to extend the photo-response of the TiO_2 to the visible region by modifying its optical properties to achieve the more efficient photocatalytic activity. Li et al. [19] prepared Fe doped TiO_2 , which has photocatalytic activity under visible light. The Fe^{3+} ion is often used as a dopant because the ionic radius (0.690 Å) is closed to Ti^{4+} (0.745 Å). Therefore, Fe^{3+} can be easily incorporated into the TiO_2 crystal lattice [19]. This study reports the preparation of $\text{SiO}_2/\text{TiO}_2\text{-Fe}$ using sugarcane bagasse ash as the new potential of a silica source. This catalyst has not been synthesized and examined in the previous research. The effect of Fe(III) addition on the properties and photocatalytic activity of $\text{SiO}_2/\text{TiO}_2$ for the degradation of Congo Red was evaluated.

■ EXPERIMENTAL SECTION

Materials

The materials used in this research were in pro-analysis qualities obtained from Sigma-Aldrich and Merck, including NaOH, HCl 37%, NH_3 25%, $\text{Ti}(\text{OCH}(\text{CH}_3)_2)_4$ 97% (TTIP), $\text{C}_2\text{H}_5\text{OH}$ 99%, $\text{FeCl}_3\cdot\text{H}_2\text{O}$ 97%, and Congo Red. Other materials were technical grade, including deionized water and sugarcane bagasse waste collected from the sugarcane factory in Bantul, Yogyakarta. All reagents were used as received without further purification.

Instrumentation

The instrumentations used in this research were Fourier Transform Infrared Spectrophotometer (Nicolet Avatar 360 IR; Shimadzu 2450), X-Ray Diffractometer

(PANalytical: X'Pert PRO 2318), Scanning Electron Microscope with Energy Dispersive X-Ray (JEOL JED-2300; Hitachi SU 3500), X-Ray Fluorescence Spectrometer (S2 PUMA), Specular Reflectance Ultraviolet-Visible Spectrometer (Shimadzu 2450), and Surface Area Analyzer (Quantachrome Nova 4200e).

Procedure

Extraction of SiO_2 from sugarcane bagasse ash

Sugarcane bagasse (1 g) was washed with 100 mL water and dried at 100 °C for 4 h. Dried sugarcane bagasse was then combusted at 1000 °C for 4 h and dispersed in 10 mL HCl 1 M for 2 h at room temperature. Furthermore, the ash treated with acid was filtered, washed with distilled water, and dried for 24 h at 80 °C. The dried ash was then dispersed in 10 mL NaOH 2 M, stirred for 4 h at 80 °C and filtered to obtain filtrate of sodium silicate solution. The sodium silicate solution was then titrated with HCl 1 M to reach pH 7.0 and form SiO_2 sol. The sol was aged for 20 h at room temperature to produce SiO_2 gel. Finally, silica gel was washed with 5 mL distilled water, filtered, and dried at 70 °C for 24 h [20].

Preparation of $\text{SiO}_2/\text{TiO}_2\text{-Fe}$, $\text{SiO}_2/\text{TiO}_2$, TiO_2

$\text{SiO}_2/\text{TiO}_2\text{-Fe}$ was prepared with a modified method from previous studies of $\text{TiO}_2\text{-Fe}$ [21] and SiO_2 from sugarcane bagasse [20]. The $\text{SiO}_2/\text{TiO}_2\text{-Fe}$ was prepared with SiO_2 to TiO_2 mass ratio of 1:1. This ratio is based on previously unpublished optimization results. The first step was extracting SiO_2 from 1 g sugarcane bagasse ash to produce SiO_2 gel. TiO_2 sol was then prepared by stirring 4 mL (13.2 mmol) TTIP, 1 mL water, 2.3 mL $\text{C}_2\text{H}_5\text{OH}$, and 0.7 mL HCl (molar ratio of 1:4:3:0.01) for 3 h. The mixture was then added with 1 mL Fe(III) solution with a varied concentration (1, 3, 5, and 7% (w/w)) at stirring for 30 min. The mixture was then sonicated for 10 min and then added to SiO_2 gel. NH_4OH solution (20 mL) was added to the mixture then sonicated for 1 h to produce $\text{SiO}_2/\text{TiO}_2\text{-Fe}$ homogeneous sol. The sol was dried at 70 °C for 24 h, and the composite obtained was calcined at 500 °C for 4 h.

$\text{SiO}_2/\text{TiO}_2$ preparation was performed with a similar procedure to the $\text{SiO}_2/\text{TiO}_2\text{-Fe}$ without the

addition of Fe. The TiO₂ was synthesized by adding 2 mL (13.2 mmol) TTIP into 20 mL ethanol solution and then added dropwise with distilled water and sonicated for 1 h. The sol was dried at 70 °C for 24 h and calcined at 500 °C for 4 h to get TiO₂ as an anatase phase.

Photocatalytic activity

Experiments were performed by mixing an aqueous solution (20 mL) of Congo Red 10 mg/L at a pH 3 with 30 mg of photocatalysts (TiO₂, SiO₂/TiO₂, and SiO₂/TiO₂-Fe) in all variations of dopant concentration (1, 3, 5, and 7%). All the reactions were performed under stirring for 90 min with various conditions: dark and under visible illumination in a closed photoreactor equipped with LED 12 W Philips lamp ($\lambda = 483\text{--}595$ nm) as the light source. Then, the photocatalyst was separated through centrifugation with the type of the centrifuge is Gemmy PLC-025. The filtrate obtained was analyzed with a UV-visible spectrophotometer with the type of GENESYS 10S. The filtrate was scanned with a wavelength from 200 to 600 nm and the optimum wavelength obtained was 561 nm. The photocatalytic degradation percentage has been calculated as

$$\text{Degradation}(\%) = \frac{C_0 - C_e}{C_0}$$

where C_0 and C_e correspond to the initial and final concentration of dye before and after photo-irradiation.

RESULTS AND DISCUSSION

SiO₂ Extraction from Sugarcane Bagasse

In this research, silica (SiO₂) was obtained from sugarcane bagasse ash and used as the matrix in SiO₂/TiO₂-Fe. Sugarcane bagasse ash was utilized as the source of silica because it has a large amount of silica content after being combusted at 1000 °C and treated with acid. Sugarcane bagasse would undergo a pyrolysis process, which will reduce the organic and inorganic contents such as K⁺ and Ca²⁺ into its oxidized form. In addition, the acid treatment caused other minerals besides SiO₂ in sugarcane bagasse ash to dissolve, and their content would decrease relatively to SiO₂. The sugarcane bagasse ash was analyzed with XRF, and the result is presented in Table 1. The major component in sugarcane bagasse ash is SiO₂ with 90.87%.

Fig. 1 displays infrared spectra of raw sugarcane bagasse, sugarcane bagasse ash, and silica. From the raw sugarcane bagasse spectrum, it could be seen there are peaks at 3416 and 1326 cm⁻¹, which indicate the stretching and bending vibration of H–O–H. In addition, there were some peaks at 2909 and 1054 cm⁻¹ stretching of Csp³–H and stretching of C–O from primary alcohol, respectively. In addition, there are also peaks at 1250 and 1730 cm⁻¹, which indicate the existence of C–O, and C=O stretching vibration, respectively [22]. According to these data, the sugarcane bagasse may contain lignin and lignocellulose. From the sugarcane bagasse ash spectrum, some peaks could be seen at 3448, 1054, 786, and 497 cm⁻¹, which indicate stretching vibration of H–O–H, Si–O–Si asymmetric stretching, Si–O–Si symmetric stretching, and bending vibration of Si–O–Si, respectively [23]. There is also a peak with low intensity at 617 cm⁻¹, which shows the characteristic of silica cristobalite. Cristobalite is formed

Table 1. Composition of sugarcane bagasse ash

Component	Content (% mass)
SiO ₂	90.87
CaO	3.060
MgO	2.077
Na ₂ O	1.186
Al ₂ O ₃	1.003

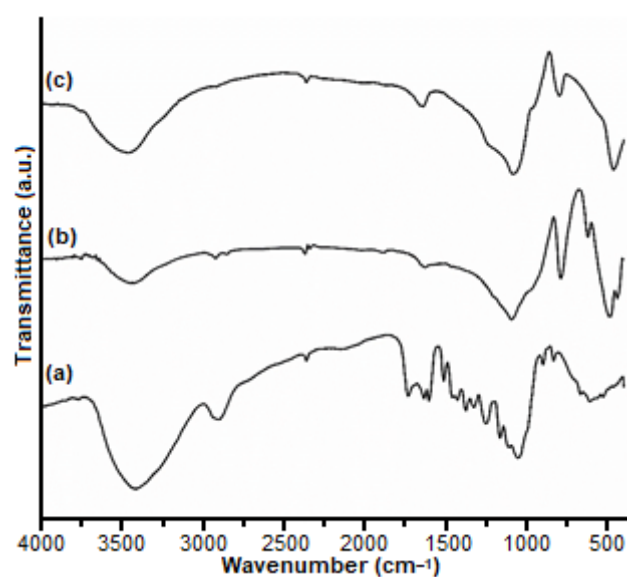


Fig 1. Infrared spectra of raw sugarcane bagasse (a), sugarcane bagasse ash (b), and extracted silica (c)

when silica is heated at 1000 °C. At this temperature, tridymite turns into cristobalite [24]. The silica spectrum shows peaks at 3467 and 1639 cm^{-1} , respectively, indicating adsorbed water's stretching and bending vibration on the SiO_2 surface. In addition, peaks at 1083, 954, and 462 cm^{-1} , indicate stretching vibration of Si–O–Si, stretching vibration of the non-bridging oxygen atom (Si–OH) [25] and bending vibration of Si–O–Si, respectively.

The X-ray diffraction pattern in Fig. 2 shows an amorphous pattern with a prominent peak at 2θ 22.16°, and a broad peak at 16–17° appears for the raw sugarcane bagasse ash. These peaks are typical peaks of cellulose corresponding to the Miller index in ICDD (International Center for Diffraction Data) number 00-003-0289 with the (hkl) values being: (-111) and (002). The XRD pattern of sugarcane bagasse ash shows peaks at 2θ 19.68, 21.83, 28.26, 31.39, and 36.07°. According to Miller's ICDD index number 00-039-1425, this is the diffraction pattern index of cristobalite with (hkl) of (101), (111), (102), and (112). Based on the diffraction pattern of silica, there is an amorphous pattern between 2θ 10–15° with a broad peak at 20.76°. There are also some sharp peaks at pada 28.16, 31.32, 40.45, 45.06, and 56.02°. This diffraction pattern was compared to Miller ICDD index number 00-003-0267, which is the diffraction pattern index of cristobalite.

Fig. 3(a) depicts an SEM image of extracted SiO_2 ; it can be explained that the surface of SiO_2 looks quite smooth even though there are some abrupt areas. Fig. 3(b) displays the SEM-EDX spectrum of SiO_2 , which shows that SiO_2 consists of O and Si elements on the material's surface. The SEM-EDX data confirm that the material is only composed of Si and O atoms as shown in Table 2.

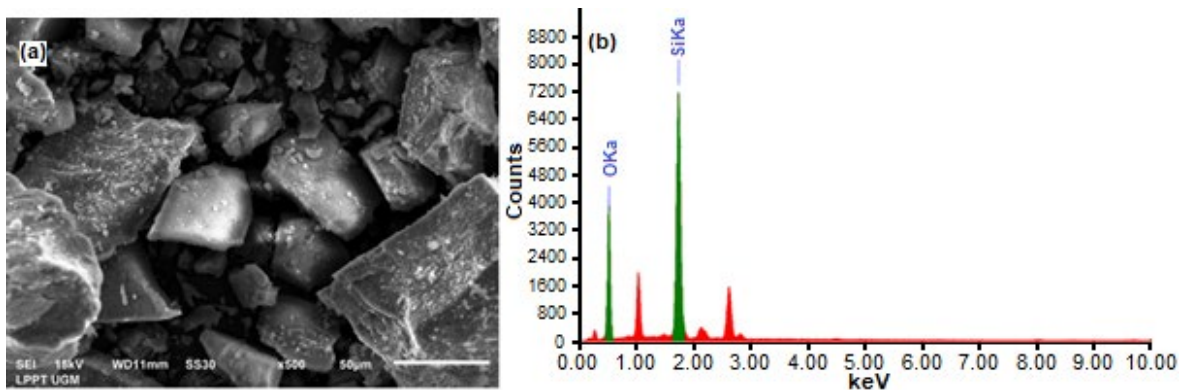


Fig 3. SEM image of SiO_2 (a) EDX spectrum of SiO_2 (b)

Characterization of $\text{SiO}_2/\text{TiO}_2\text{-Fe}$

Fig. 4 displays the infrared spectra of $\text{SiO}_2/\text{TiO}_2$ and $\text{SiO}_2/\text{TiO}_2\text{-Fe}$ with various dopant concentrations. The spectra show that in all variations, absorption peaks appear at 410–495, 500–600, 920–927, 1026–1050, and 2360–2370 cm^{-1} . These peaks indicate respectively the stretching vibration of Si–O–Si, bending vibration of Ti–O–Ti, stretching vibration of Ti–O–Si, bending vibration of Si–O–Si, and stretching vibration of Ti–O–Ti. Sharp

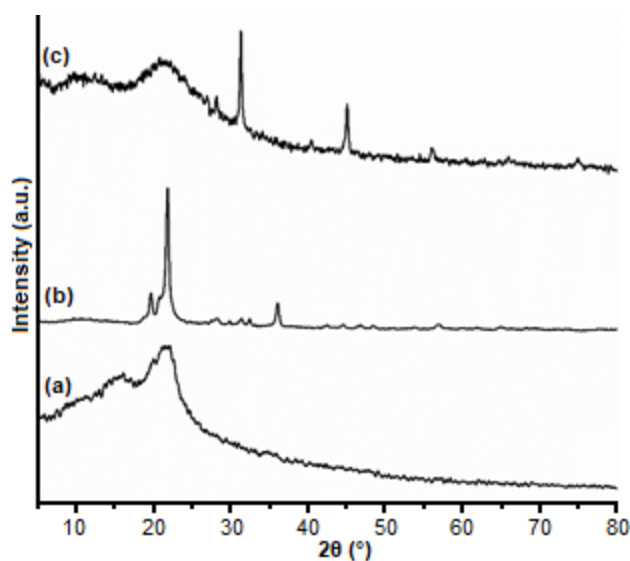


Fig 2. X-ray diffraction pattern of raw sugarcane bagasse (a), sugarcane bagasse ash (b), and extracted silica (c)

Table 2. Elements composition on the surface of SiO_2

Element	Atom%
O	79.94
Si	29.06
Total	100.00

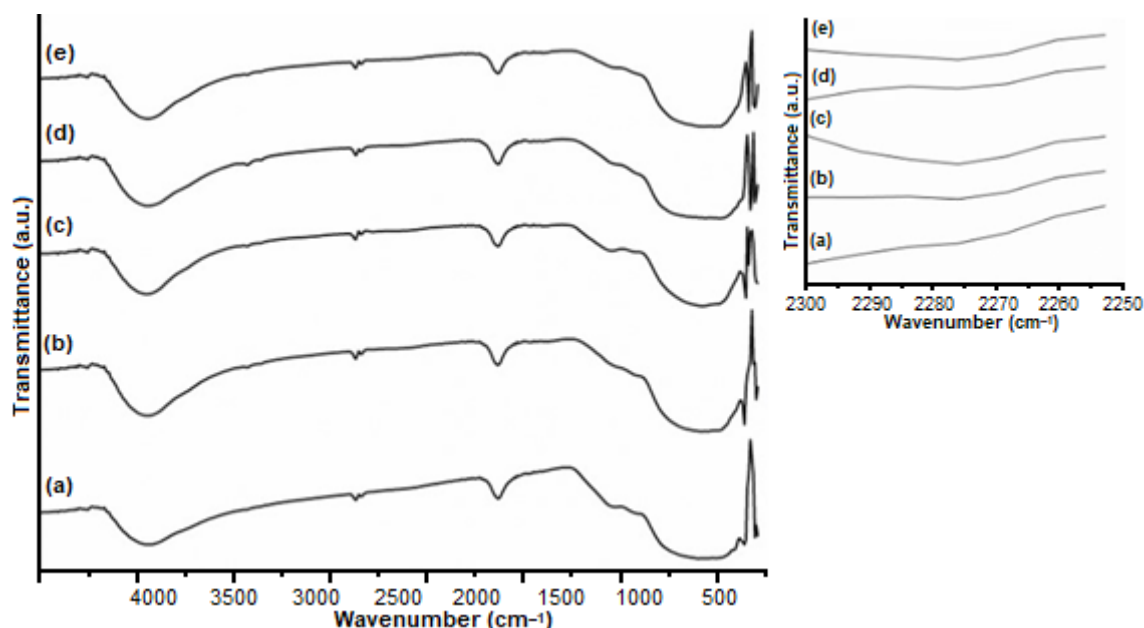


Fig 4. Infrared spectra of $\text{SiO}_2/\text{TiO}_2$ (a), and $\text{SiO}_2/\text{TiO}_2\text{-Fe}$ 1% (b), 3% (c), 5% (d), 7% (e)

peaks at 3400 and 1600 cm^{-1} also appear, indicating H–O–H's stretching and bending vibration. The addition of Fe(III) as a dopant gives a new peak at 2200 cm^{-1} with low intensity, as can be seen in inset spectra in Fig. 4. This peak is a characteristic of Ti–O–Fe vibration that Fe inserted into the TiO_2 crystal lattice [26].

Fig. 5 presents the X-ray diffraction pattern of $\text{SiO}_2/\text{TiO}_2$ and $\text{SiO}_2/\text{TiO}_2\text{-Fe}$ with various dopant concentrations of Fe(III). There are characteristic peaks of silica cristobalite and anatase of $\text{SiO}_2/\text{TiO}_2$ and $\text{SiO}_2/\text{TiO}_2\text{-Fe}$ samples. The peaks of silica cristobalite are shown at 2θ 28, 31, 40, 45, 56° according to ICDD number 00-003-0267. TiO_2 anatase is revealed at 25, 48, 75° according to ICDD number 00-002-0406. Table 3 shows that at 2θ of 25° of the $\text{SiO}_2/\text{TiO}_2\text{-Fe}$ is shifted toward a smaller 2θ than $\text{SiO}_2/\text{TiO}_2$. It denotes Fe^{3+} was successfully doped in interstitial mode, causing the distance between planes of $\text{SiO}_2/\text{TiO}_2\text{-Fe}$ to be greater than $\text{SiO}_2/\text{TiO}_2$. The Fe^{3+} radius is smaller than the Ti^{4+} radius, making it possible for Fe^{3+} ions to enter the crystal cell of TiO_2 on the interstitial mode within the crystal lattice [27]. It is noted that crystal size continues to decrease as the Fe^{3+} concentration increase implying the doped Fe^{3+} could inhibit the grain growth of TiO_2 .

The TiO_2 and $\text{TiO}_2\text{-Fe}$ were dispersed into the SiO_2

matrix to achieve a more significant surface area. Table 3 shows that $\text{SiO}_2/\text{TiO}_2$ has a greater surface area ($72.59\text{ m}^2/\text{g}$) than TiO_2 ($20.26\text{ m}^2/\text{g}$). It confirms that dispersing TiO_2 into the SiO_2 matrix would increase the surface area due to the presence of porous SiO_2 , which has a high specific surface area [28]. The $\text{SiO}_2/\text{TiO}_2\text{-Fe}$ also has a greater surface area than the undoped material. Therefore, Fe dopant can inhibit the growth of

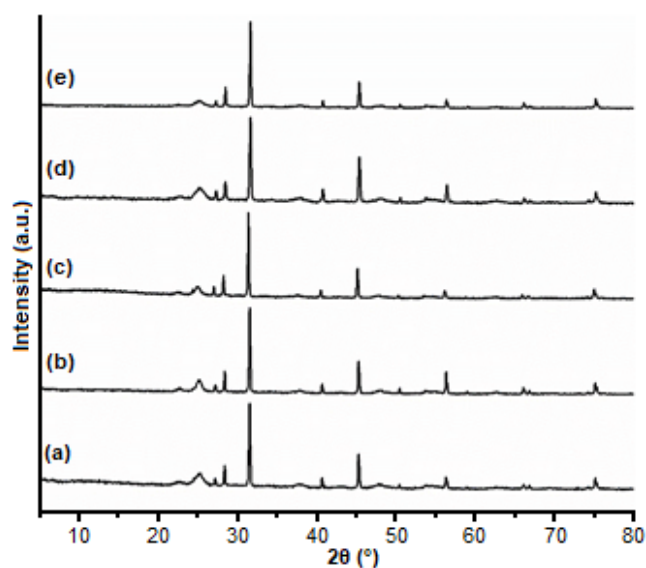


Fig 5. X-ray diffraction pattern of $\text{SiO}_2/\text{TiO}_2$ (a), and $\text{SiO}_2/\text{TiO}_2\text{-Fe}$ 1% (b), 3% (c), 5% (d), 7% (e)

TiO₂ crystal, crystal, reducing the crystal size and increasing the material surface area [29]. This fact correlates to the crystallite size data shown in Table 4 where SiO₂/TiO₂-Fe 5% has a smaller size than SiO₂/TiO₂.

The EDX was also carried out to determine the elements in SiO₂/TiO₂ and SiO₂/TiO₂-Fe. The EDX data of SiO₂/TiO₂ shows that SiO₂/TiO₂ contains O, Ti, and Si, meanwhile SiO₂/TiO₂-Fe consists of O, Ti, Si, and Fe. The element composition of both materials can be seen in Table 5. The result denotes that the surface of the materials is dominated by Ti, giving a better photocatalytic performance.

Fig. 6 shows SiO₂/TiO₂ and SiO₂/TiO₂-Fe SEM images, which show that compared to the SiO₂ surface, both materials have rougher surfaces caused by TiO₂ and TiO₂-Fe particles dispersed on the SiO₂ surface. SEM mapping was conducted to see the distribution of the atoms on the surface of SiO₂/TiO₂ (Fig. 7(a)) and SiO₂/TiO₂-Fe (Fig. 7(b)). It can be seen that Ti and Si atoms occupy the same position on both materials, indicating the formation of SiO₂/TiO₂ composite. Ti and Fe atoms also occupy the same position, indicating Fe doping into the TiO₂ crystal lattice.

Characterization using the SR UV-Visible method is aimed to determine the material's bandgap energy (E_g). Fig. 8 reveals a shift of absorption wavelength toward the visible light region with an increasing concentration of Fe. The E_g was calculated from the data using the Tauc plot. Table 6 demonstrates that SiO₂/TiO₂ has a slightly higher E_g than that of TiO₂. It might be caused by the quantum size effect, which inhibits the TiO₂ crystal growth [30]. The TiO₂ E_g 3.15 eV corresponds to the results reported

by Aguado [31] that TiO₂ anatase has the E_g value in the range of 3.08–3.35 eV. The E_g of the doped materials tends to decrease as the Fe concentration increase. It occurs because the distance between the valence and conduction bands is getting smaller due to forming a new energy level originating from the d orbitals of Fe metal dopant below the conduction band. The distance of the new energy level with the formed conduction band becomes smaller, and electron transfer requires lower energy.

Table 3. The surface area of materials

Material	SBET (m ² /g)
TiO ₂	10.26
TiO ₂ /SiO ₂	72.59
TiO ₂ /SiO ₂ -Fe 5%	108.6

Table 4. The d-space and crystallite size of materials

Material	2θ (°)	d (Å)	D (nm)
TiO ₂ /SiO ₂	25.38	3.507	19.34
TiO ₂ /SiO ₂ -Fe 1%	25.22	3.528	15.75
TiO ₂ /SiO ₂ -Fe 3%	24.94	3.567	11.81
TiO ₂ /SiO ₂ -Fe 5%	25.22	3.528	10.67
TiO ₂ /SiO ₂ -Fe 7%	25.32	3.515	10.64

Table 5. Elements composition on the surface of SiO₂/TiO₂ and SiO₂/TiO₂-Fe

Material	Element	Atom%
SiO ₂ /TiO ₂	O	67.97
	Si	3.97
	Ti	28.06
SiO ₂ /TiO ₂ -Fe 5%	O	67.36
	Si	2.21
	Ti	28.58
	Fe	1.85

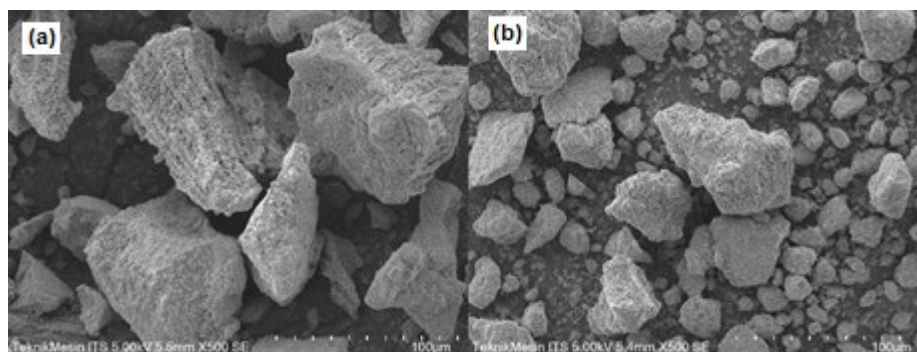


Fig 6. SEM image of SiO₂/TiO₂ (a) and SiO₂/TiO₂-Fe (b)

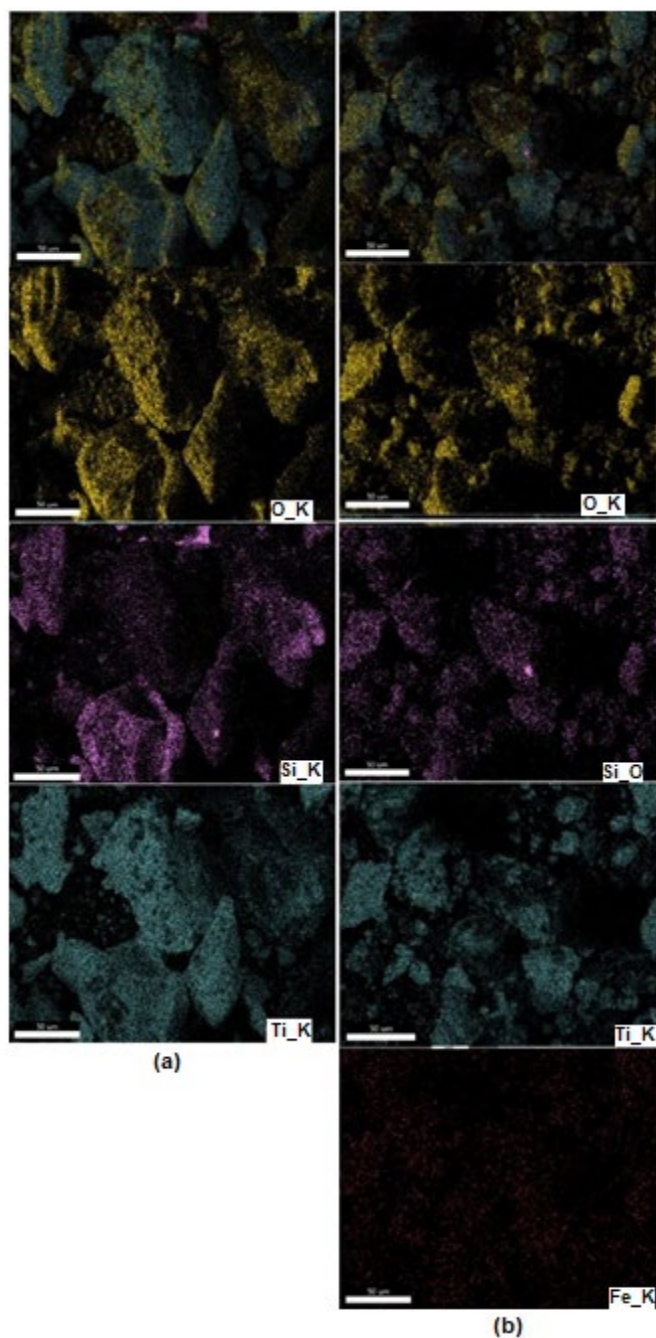


Fig 7. Elements mapping on the $\text{SiO}_2/\text{TiO}_2$ (a) and $\text{SiO}_2/\text{TiO}_2\text{-Fe}$ 5% (b) surface

It is noted that E_g is shifted towards higher energy at a dopant concentration of 7%. It might be caused by the Burstein-Moss effect, which stated that when the concentration of dopants is too abundant, the electrons occupying the conduction band will be excess so that it can push the Fermi level up. This increased fermi level results in an increase in the bandgap energy [32].

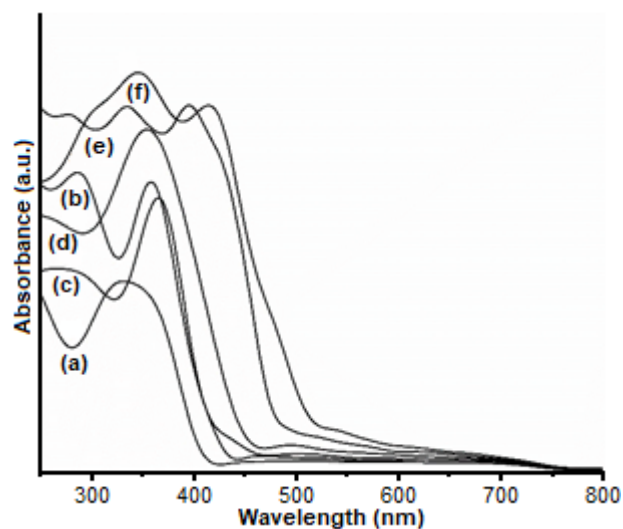


Fig 8. Specular Reflectance UV-Visible Spectra of TiO_2 (a), $\text{SiO}_2/\text{TiO}_2$ (b), $\text{SiO}_2/\text{TiO}_2\text{-Fe}$ 1% (c), $\text{SiO}_2/\text{TiO}_2\text{-Fe}$ 3% (d), $\text{SiO}_2/\text{TiO}_2\text{-Fe}$ 5% (e), and $\text{SiO}_2/\text{TiO}_2\text{-Fe}$ 7% (f)

Table 6. Bandgap energy of prepared material

Material	E_g (eV)
TiO_2	3.15
$\text{SiO}_2/\text{TiO}_2$	3.16
$\text{SiO}_2/\text{TiO}_2\text{-Fe}$ 1%	3.06
$\text{SiO}_2/\text{TiO}_2\text{-Fe}$ 3%	2.93
$\text{SiO}_2/\text{TiO}_2\text{-Fe}$ 5%	2.63
$\text{SiO}_2/\text{TiO}_2\text{-Fe}$ 7%	2.67

Photocatalytic Activity of $\text{SiO}_2/\text{TiO}_2\text{-Fe}$

The photocatalytic activity of $\text{SiO}_2/\text{TiO}_2\text{-Fe}$ was examined to degrade the Congo Red in the aqueous solution. Fig. 9 shows the photocatalytic activity under visible light illumination. The Fe doped $\text{SiO}_2/\text{TiO}_2$ material obtained the highest percentage of Congo Red degradation with a concentration of Fe(III) 5% (98.18%). It is related to the obtained E_g where $\text{SiO}_2/\text{TiO}_2\text{-Fe}$ (5%) has the lowest E_g value of 2.39 eV, requiring the smallest energy to excite electrons from the valence band to the conduction band. On the other hand, the $\text{SiO}_2/\text{TiO}_2\text{-Fe}$ photocatalysts with dopant concentrations of 1, 3, and 7% have larger E_g values shown in Table 6, so that it requires greater energy to excite the electrons. Thus, resulting in lower percentage degradation, as can be seen in Fig. 9. Even though some of these photocatalysts have a higher E_g value, they are still responsive to visible light.

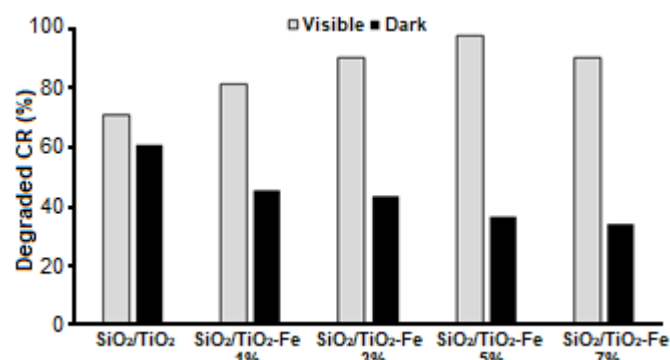
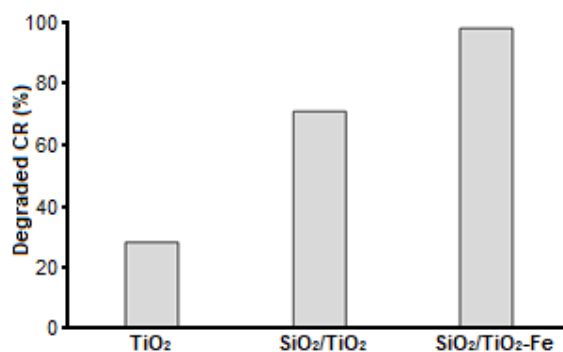
Table 7. Comparison of Congo Red degradation percentage with reported studies

Catalyst	Initial dye conc. (mg/L)	Light source	Time (min)	Degradation (%)	Ref
TiO ₂	4	58 W UV lamp	30	64.72	[33]
ZrO ₂ /TiO ₂ /ZnO	10	8 W UV lamp	15	97	[34]
TiO ₂ -Fe	20	250 W Xenon lamp	60	54.16	[35]
PVA/TiO ₂ /Chi/Chl	10	W70 LED lamp	210	94	[36]
Mn-TiO ₂ /Ti	1	150 W visible lamp	60	75.48	[37]
SiO ₂ /TiO ₂ -Fe	10	12 W LED lamp	90	98.18	This study

According to Fig. 9, it can be seen that SiO₂/TiO₂-Fe photocatalysts can reduce the concentration of Congo Red in dark conditions with no external energy source. In this condition, the reduction of Congo Red concentration is not caused by photocatalytic degradation but adsorption. The adsorption could occur due to the active sites on the surface of the photocatalysts. This process is recognized as decolorization. The SiO₂ can act as a suitable adsorbent that provides an adsorption site to support TiO₂ in capturing more target molecules.

Fig. 10 shows that SiO₂/TiO₂-Fe with Fe(III) 5% concentration gave the highest photocatalytic activity than pure TiO₂ and undoped SiO₂/TiO₂. The SiO₂/TiO₂-Fe can degrade more Congo Red due to the contribution of SiO₂, which acts as an adsorbent and gives a greater surface area as a result of TiO₂ dispersion into the SiO₂ matrix. The dopant added is responsive to visible light and improves photocatalyst's performance in the visible light region. The percentage degradation of SiO₂/TiO₂ is lower than SiO₂/TiO₂-Fe in visible light illumination due to the E_g compatibility. It can be concluded that SiO₂/TiO₂-Fe will be more effectively used as a photocatalyst than unmodified TiO₂.

Until the present day, there has not been any report of SiO₂/TiO₂-Fe with extracted silica from sugarcane bagasse ash for photocatalytic degradation of Congo Red. Therefore, earlier reported studies including various photocatalysts were compared with this study for Congo Red degradation. The comparisons data can be seen in Table 7. Compared to all the photocatalysts used, SiO₂/TiO₂-Fe has the highest activity within a relatively short period. Thus, it suggests that SiO₂/TiO₂-Fe may be a good choice for wastewater treatment.

**Fig 9.** Percentage degradation of Congo Red (CR) catalyzed by SiO₂/TiO₂ and SiO₂/TiO₂-Fe under visible light and dark condition**Fig 10.** Percentage degradation of Congo Red (CR) catalyzed by TiO₂, SiO₂/TiO₂, and SiO₂/TiO₂-Fe 5% under visible light irradiation

CONCLUSION

Silica was successfully extracted from sugarcane bagasse ash with a content of 90.87%. SiO₂/TiO₂-Fe photocatalysts were also successfully synthesized. The addition of SiO₂ gives a higher surface area on the SiO₂/TiO₂-Fe compared to the unmodified TiO₂. Furthermore, Fe(III) modification on SiO₂/TiO₂

influences the bandgap energy of TiO₂, resulting in a lower value of E_g from 3.15 to 2.63 eV. Therefore, the SiO₂/TiO₂-Fe can be used as a photocatalyst responsive to visible light for Congo Red degradation under visible light exposure. The Fe doped SiO₂/TiO₂ with a dopant concentration of 5% can degrade 10 mg/L of Congo Red dye solution with a degradation yield of 98.18% under the condition of pH 3, under visible light illumination for 90 min. This finding led to a conclusion of possible new materials for wastewater treatment.

■ ACKNOWLEDGMENTS

The authors acknowledge to Faculty of Mathematics and Natural Sciences, Universitas Gadjah Mada, for the financial support of this research (DAMAS 2021 internal research grant, with contract number: 163/J01.1.28/PL.06.02/2021).

■ REFERENCES

- [1] Hernández-Zamora, M., and Martínez-Jerónimo, F., 2019, Congo red dye diversely affects organisms of different trophic levels: A comparative study with microalgae, cladocerans, and zebrafish embryos, *Environ. Sci. Pollut. Res.*, 26 (12), 11743–11755.
- [2] Batool, M., Qureshi, M.Z., Hashmi, F., Mehboob, N., and Shah, A.S., 2019, Congo red azo dye removal and study of its kinetics by aloe vera mediated copper oxide nanoparticles, *Indones. J. Chem.*, 19 (3), 626–637.
- [3] Lindu, M., 2008, The effects of gradient velocity and detention time to coagulation– flocculation of dyes and organic compound in deep well water, *Indones. J. Chem.*, 8 (2), 146–150.
- [4] Karamah, E.F., and Nurcahyani, P.A., 2019, Degradation of blue KN-R dye in batik effluent by an advanced oxidation process using a combination of ozonation and hydrodynamic cavitation, *Indones. J. Chem.*, 19 (1), 41–47.
- [5] Zargoosh, K., Rostami, M., and Aliabadi, H.M., 2020, Eu²⁺- and Nd³⁺-doped CaAl₂O₄/WO₃/polyester nanocomposite as a sunlight-activated photocatalyst for fast removal of dyes from industrial wastes, *J. Mater. Sci.: Mater. Electron.*, 31 (14), 11482–11495.
- [6] Liu, L., and Li, Y., 2014, Understanding the reaction mechanism of photocatalytic reduction of CO₂ with H₂O on TiO₂-based photocatalysts: A review, *Aerosol Air Qual. Res.*, 14 (2), 453–469.
- [7] Tangale, N.P., Niphadkar, P.S., Samuel, V., Deshpande, S.S., Joshi, P.N., and Awate, S.V., 2016, Synthesis of Sn-containing anatase (TiO₂) by sol-gel method and their performance in catalytic water splitting under visible light as a function of tin content, *Mater. Lett.*, 171, 50–54.
- [8] Chen, J., Qiu, F., Xu, W., Cao, S., and Zhu, H., 2015, Recent progress in enhancing photocatalytic efficiency of TiO₂-based materials, *Appl. Catal., A*, 495, 131–140.
- [9] Manurung, P., Situmeang, R., Ginting, E., and Pardede, I., 2015, Synthesis and characterization of titania-rice husk silica composites as photocatalyst, *Indones. J. Chem.*, 15 (1), 36–42.
- [10] Rovani, S., Santos, J.J., Corio, P., and Fungaro, D.A., 2018, Highly pure silica nanoparticles with high adsorption capacity obtained from sugarcane waste ash, *ACS Omega*, 3 (3), 2618–2627.
- [11] Fonseca-Cervantes, O.R., Pérez-Larios, A., Romero Arellano, V.H., Sulbaran-Rangel, B., and Guzmán González, C.A., 2020, Effects in band gap for photocatalysis in TiO₂ support by adding gold and ruthenium, *Processes*, 8 (9), 1032.
- [12] Wan, H., Yao, W., Zhu, W., Tang, Y., Ge, H., Shi, X., and Duan, T., 2018, Fe-N co-doped SiO₂@TiO₂ yolk-shell hollow nanospheres with enhanced visible light photocatalytic degradation, *Appl. Surf. Sci.*, 444, 355–363.
- [13] D'Amato, C.A., Giovannetti, R., Zannotti, M., Rommozzi, E., Minicucci, M., Gunnella, R., and Di Cicco, A., 2018, Band gap implications on nano-TiO₂ surface modification with ascorbic acid for visible light-active polypropylene coated photocatalyst, *Nanomaterials*, 8 (8), 599.
- [14] Liu, J., Li, Y., Ke, J., Wang, S., Wang, L., and Xiao, H., 2018, Black NiO-TiO₂ nanorods for solar photocatalysis: Recognition of electronic structure and reaction mechanism, *Appl. Catal., B*, 224, 705–714.

- [15] Niu, X., Yan, W., Shao, C., Zhao, H., and Yang, J., 2019, Hydrothermal synthesis of Mo-C co-doped TiO₂ and coupled with fluorine-doped tin oxide (FTO) for high-efficiency photodegradation of methylene blue and tetracycline: Effect of donor-acceptor passivated co-doping, *Appl. Surf. Sci.*, 466, 882–892.
- [16] El Mragui, A., Logvina, Y., da Silva, L.P., Zegaoui, O., and da Silva, J.C.G.E., 2019, Synthesis of Fe⁻ and co-doped TiO₂ with improved photocatalytic activity under visible irradiation toward carbamazepine degradation, *Materials*, 12 (23), 3874.
- [17] Raza, W., Haque, M.M., Muneer, M., Fleisch, M., Hakki, A., and Bahnemann, D., 2015, Photocatalytic degradation of different chromophoric dyes in aqueous phase using La and Mo doped TiO₂ hybrid carbon spheres, *J. Alloys Compd.*, 632, 837–844.
- [18] Wu, J.C.S., and Chen, C.H., 2004, A visible-light response vanadium-doped titania nanocatalyst by sol-gel method, *J. Photochem. Photobiol., A*, 163 (3), 509–515.
- [19] Li, Z., Shen, W., He, W., and Zu, X., 2008, Effect of Fe-doped TiO₂ nanoparticle derived from modified hydrothermal process on the photocatalytic degradation performance on methylene blue, *J. Hazard. Mater.*, 155 (3), 590–594.
- [20] Norsuraya, S., Fazlena, H., and Norhasyimi, R., 2016, Sugarcane bagasse as a renewable source of silica to synthesize Santa Barbara Amorphous-15 (SBA-15), *Procedia Eng.*, 148, 839–846.
- [21] Anwar, D.I., and Mulyadi, D., 2015, Synthesis of Fe-TiO₂ composite as a photocatalyst for degradation of methylene blue, *Procedia Chem.*, 17, 49–54.
- [22] Kumar, A., Negi, Y.S, Choudhary, V., and Bhardwaj, N.K., 2014, Characterization of cellulose nanocrystals produced by acid-hydrolysis from sugarcane bagasse as agro-waste, *J. Mater. Phys. Chem.*, 2 (1), 1–8.
- [23] Worathanakul, P., Payubnop, W., and Muangpet, A., 2009, Characterization for post-treatment effect of bagasse ash for silica extraction, *World Acad. Sci. Eng. Technol.*, 3 (8), 398–400.
- [24] Dapiaggi, M., Pagliari, L., Pavese, A., Sciascia, L., Merli, M., and Francescon, F., 2015, The formation of silica high temperature polymorphs from quartz: Influence of grain size and mineralising agents, *J. Eur. Ceram. Soc.*, 35 (16), 4547–4555.
- [25] Rahman, N.A., Widhiana, I., Juliastuti, S.R., and Setyawan, H., 2015, Synthesis of mesoporous silica with controlled pore structure from bagasse ash as a silica source, *Colloids Surf., A*, 476, 1–7.
- [26] Luu, C.L., Nguyen, Q.T., and Ho, ST, 2010, Synthesis and characterization of Fe-doped TiO₂ photocatalyst by the sol-gel method, *Adv. Nat. Sci.: Nanosci. Nanotechnol.*, 1, 015008.
- [27] Yang, Y., Yu, Y., Wang, J., Zheng, W., and Cao, Y., 2017, Doping and transformation mechanisms of Fe³⁺ ions in Fe-doped TiO₂, *CrystEngComm*, 19 (7), 1100–1105.
- [28] Huynh, N.D.T., Vo, K.D., Nguyen, T.V., and Le, M.V., 2019, Enhancing the photoactivity of TiO₂/SiO₂ monolithic catalyst and its reusability for wastewater treatment, *MATEC Web Conf.*, 268, 07005.
- [29] Safari, M., Talebi, R., Rostami, M.H., Nikazar, M., and Dadvar, M., 2014, Synthesis of iron-doped TiO₂ for degradation of reactive orange 16, *J. Environ. Health Sci. Eng.*, 12 (1), 19.
- [30] Othman, S.H., Rashid, S.A., Mohd Ghazi, T.I., and Abdullah, N., 2011, Fe-doped TiO₂ nanoparticles produced via MOCVD: Synthesis, characterization, and photocatalytic activity, *J. Nanomater.*, 2011, 571601.
- [31] Aguado, J., van Grieken, R., López-Muñoz, M.J., and Marugán, J., 2006, A comprehensive study of the synthesis, characterization and activity of TiO₂ and mixed TiO₂/SiO₂ photocatalysts, *Appl. Catal., A*, 312, 202–212.
- [32] Munir, S., Shah, S.M., Hussain, H., and Ali khan, R., 2016, Effect of carrier concentration on the optical band gap of TiO₂ nanoparticles, *Mater. Des.*, 92, 64–72.
- [33] Harun, N.S., Rahman, M.N.A., Kamarudin, W.F.W., Irwan, Z., Muhammad, A., Akhir, N.E.F.M., and Yaafar, M.R., 2018, Photocatalytic degradation of Congo red dye based on titanium

- dioxide using solar and UV lamp, *J. Fundam. Appl. Sci.*, 10 (1S), 832–846.
- [34] Seyedi-Chokanlou, T., Aghabeygi, S., Molahasani, N., and Abrinaei, F., 2021, Applying Taguchi method to optimize the synthesis conditions of $ZrO_2/TiO_2/ZnO$ nanocomposite for high-performance photodegradation of Congo red, *Iran. J. Catal.*, 11 (1), 49–58.
- [35] Kaya, D., and Türkten, N., 2020, Preparation of doped TiO_2 photocatalysts and their decolorization efficiencies under solar light, *J. Eng. Sci. Des.*, 8 (3), 655–663.
- [36] Jo, W.K., and Tayade, R.J., 2014, New generation energy-efficient light source for photocatalysis: LEDs for environmental applications, *Ind. Eng. Chem. Res.*, 53 (6), 2073–2084.
- [37] Nurdin, M., Maulidiyah, M., Syahputra, R.A., Salim, L.O.A., Wati, I., Irwan, I., and Mustapa, F., 2021, Degradation test of organic congo red compounds using $Mn-TiO_2/Ti$ electrode by photocatalytic under the UV-visible irradiation, *J. Phys.: Conf. Ser.*, 1899, 012047.